analytical chemistry

Article

pubs.acs.org/ac

Continuous Microfluidic Particle Separation via Elasto-Inertial Pinched Flow Fractionation

Xinyu Lu and Xiangchun Xuan*

Department of Mechanical Engineering, Clemson University, Clemson, South Carolina 29634-0921, United States

Supporting Information

ABSTRACT: Many of the fluids encountered in chemical and biomedical applications exhibit non-Newtonian behavior. However, the majority of current particle separation methods have been demonstrated in Newtonian fluids only. This work presents an experimental study of continuous particle separation in viscoelastic solutions via a combined action of elastic and inertial lift forces, which we term elasto-inertial pinched flow fractionation (eiPFF). The parametric effects on eiPFF are systematically investigated in terms of dimensionless numbers. It is found that eiPFF offers much higher particle throughput and separation resolution than the traditional steric effects-based PFF. Moreover, eiPFF works most efficiently when the Reynolds number, *Re*, is of order 1 and hence fills perfectly into the gap of our recently proposed inertia-enhanced PFF (iPFF) technique (*Anal. Chem.* **2015**, *87*, 4560−4565) that favors *Re* of the order 10 or more. However, the particle separation via eiPFF does not increase monotonically with the elasticity number at higher polymer concentrations and is strongly affected by the aspect ratio of channel width to height, both of which have not been previously reported. More surprisingly, the elasto-inertial deflection of small particles can be even greater than that of large particles in a high-aspect-ratio channel for *Re* less than 1.

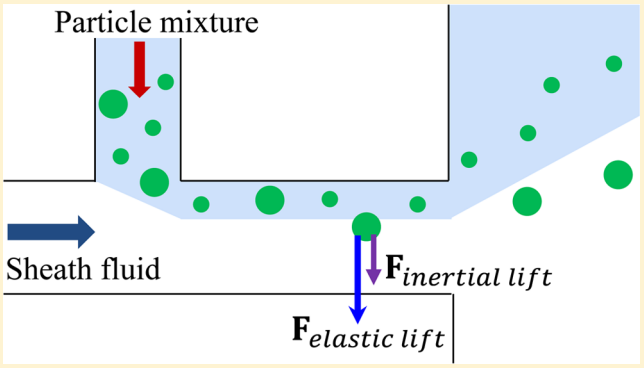

In the past 2 decades, microfluidic devices have become an attractive platform for many chemical and biomedical applications due to their enhanced efficiency and accuracy at a reduced cost.[1] Separating target particles (synthetic or biological) from a mixture in a continuous label-free manner is often a necessary step in these lab-on-a-chip applications.[2] It can be implemented based on the differences in intrinsic particle properties such as size, shape, or deformability through either an externally imposed or an internally induced force field.[3] The former type of *active* separation methods has been achieved by the use of electric,[4] optical,[5] acoustic,[6] or magnetic[7] field-induced cross-stream phoretic motions. Additionally, a variety of *passive* separation methods have been developed which exploit the confinement-induced electric or hydrodynamic force to manipulate particles toward differential equilibrium positions.[8] This type of approach covers insulator-based dielectrophoresis (iDEP),[9] deterministic lateral displacement (DLD),[10] hydrodynamic filtration,[11] hydrophoresis,[12] split-flow thin-cell fractionation (SPLITT),[13] pinched flow fractionation (PFF),[14] and inertial microfluidics,[15] etc. However, all these continuous particle separation methods have thus far been demonstrated in Newtonian fluids only.

As a matter of fact, many of the fluids that are encountered in practical microfluidic applications like polymeric solutions and bodily fluids (e.g., blood and saliva) are complex and can exhibit strong non-Newtonian behaviors such as shear thinning and viscoelasticity.[16−18] Early studies of particle motion in non-Newtonian fluids can be dated back to half a century ago,[19,20] which are mostly concerned with the particle sedimentation in a stationary fluid[21] or the particle migration in a pipe flow.[22] In the former situation, anomalous particle motion has been reported such as velocity overshoot, oscillation, and even reversal[23] due to the evolution of a negative wake.[24] For particles in viscoelastic pipe/slit flows, inward migration to the centerline has been experimentally observed,[25−27] which, as explored both theoretically[28] and numerically,[29,30] arises from the normal stress difference in the fluid. However, the effect of shear thinning can cause particles to migrate away from the centerline at increased flow rates.[31,32]

Recent studies of particle motion in non-Newtonian fluids have been shifted to rectangular microchannels that are easily available with state-of-the-art microfabrication techniques.[33] The involving flows are three-dimensional, wherein particles have been demonstrated to migrate toward multiple equilibrium positions including the centerline and the four corners.[34,35] This cross-stream particle migration to the regions of low shear rate is again a result of the normal stress difference in a viscoelastic fluid. The equilibrium positions can be reduced to only one along the channel centerline by the combined

Received: April 16, 2015
Accepted: May 25, 2015
Published: May 25, 2015

DOI: 10.1021/acs.analchem.5b01432
Anal. Chem. 2015, 87, 6389−6396

action of elastic and inertial effects,[36] which, however, is still strongly influenced by the fluid rheology.[37,38] Such a three-dimensional focusing effect has been demonstrated for a variety of (bio)particles and can remain effective at extremely high flow rates in a hyaluronic acid-based weakly elastic fluid.[39] It has also been utilized to selectively enrich and filter the larger particles from a particle mixture.[40] In addition, similar single-line particle focusing has been observed in viscoelastic flows through both a rectangular microchannel with side-wells[41] and a spiral microchannel.[42]

Besides aligning particles in planar microchannels for detecting and analyzing purposes,[43,44] the cross-stream particle migration in viscoelastic flows has also been demonstrated to separate particles in few recent studies. Yang et al.[45] reported that fresh red blood cells in a polyvinylpyrrolidone (PVP)-based phosphate buffered saline (PBS) solution can be directed toward the centerline of a straight square microchannel by the cell deformability-induced lift.[46] In contrast, rigidified red blood cells are mostly entrained along the corners due to the fluid viscoelasticity-induced lift under negligible inertia. The authors further utilized this phenomenon to isolate white blood cells (which are more rigid than red blood cells) from dilute whole blood with a high enrichment ratio.[45] Nam et al.[47] developed a simple method that exploits the particle size-dependence of elastic and inertial lift forces in viscoelastic fluids to continuously separate large particles from a sheath flow-focused particle mixture solution near the walls. This method was demonstrated to sort platelets from dilute whole blood in a poly(ethylene oxide) (PEO)-based PBS solution with a purity of close to 99.9%. A similar idea was later employed by Kang et al.[26] to implement a continuous separation of multiple polystyrene particles in an extremely dilute DNA solution.

The continuous particle separation method developed by Nam et al.[47] is similar to PFF[14] in configuration and depends on the combined action of elastic and inertial lift forces in a viscoelastic fluid, so we use the term elasto-inertial pinched flow fractionation (eiPFF). As compared to inertial microfluidics,[15,48] eiPFF is able to separate much smaller particles such as 1−2 μm in diameter[26] and can even potentially separate submicrometer particles[34] though at a smaller throughput. Moreover, it has the capability of separating complex samples (e.g., quaternary mixture of particles[26]) and works for biological cells via the use of biocompatible polymer solutions (e.g., PVP[45] and hyaluronic acid[39]). Since a direct numerical simulation of particle motion in viscoelastic fluids is currently still very challenging, this work presents a systematic experimental study of the parametric effects on continuous particle separation via eiPFF. The aim is to acquire a comprehensive understanding of the important factor(s) that may impact eiPFF and provide a useful guidance for future design and control of this novel microfluidic separation technique.

EXPERIMENTAL SECTION

Preparation of Particle Suspensions. Polystyrene spheres (Thermo Scientific) of 3.1 μm- and 9.9 μm-diameter (referred to hereafter as 3 and 10 μm for brevity) were used in the separation experiments. They were mixed at an approximately 2:1 number density ratio and resuspended in aqueous Newtonian and non-Newtonian fluids to a final concentration of about 10^7 particles per milliliter. The Newtonian fluid was prepared by mixing 21 wt % glycerol (Fisher Scientific) with water (Fisher Scientific) to match the mass density of polystyrene particles (1.05 g/cm^3).[49] The non-Newtonian fluids were prepared by dissolving PEO powder (Sigma-Aldrich, molecular weight $M_w = 2 \times 10^6$ Da) into the glycerol (21 wt %)/water solution at the concentrations of 500, 1000, and 2000 ppm, respectively. The properties of the prepared Newtonian and non-Newtonian fluids at 20 °C (the operation temperature of all experiments) are summarized in Table 1. The process for determining the relaxation times are provided in the Supporting Information.

Table 1. Properties of the 21 wt % Glycerol/Water-Based Newtonian and Non-Newtonian Fluids Used in Experiments

		Non-Newtonian (c, ppm PEO)		
fluid properties (at 20 °C)	Newtonian	500	1000	2000
density ρ (g/cm^3)	1.05	1.05	1.05	1.05
zero-shear viscosity η_0 (mPa s)	1.8	2.8	4.0	10.6
overlap concn c^* (ppm)		858	858	858
concn ratio c/c^*		0.58	1.17	2.33
Zimm relaxation time, λ_{Zimm} (ms)		0.6	0.6	0.6
effective relaxation time, λ_e (ms)		7.9	12.4	19.5

Experimental Setup. Figure 1 shows a picture of the asymmetric T-shaped microchannel used in experiments, which

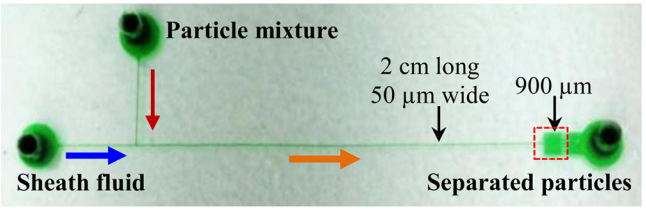

Figure 1. Top-view picture of the asymmetric T-shaped microchannel (filled with green food dye for clarity) used in experiments. The block arrows indicate the flow directions of the sheath fluid (which is the pure suspending medium of the particle mixture) and particle mixture for particle separation, which is visualized at the 900 μm-wide expansion region at the end of the 2 cm-long, 50 μm-wide main-branch (highlighted by a dashed-box).

was fabricated in polydimethylsiloxane (PDMS) using the standard soft lithography method.[50] The channel has a 2 cm-long main-branch and two 4 mm-long side-branches with a uniform width of 50 μm. There is a 900-μm wide, 2 mm-long expansion at the end of the main-branch for enhancing and visualizing the particle separation. Three depths of channels were used for the purpose of examining the effect of channel aspect ratio on particle separation, which are 25, 40, and 100 μm, respectively. The prepared sheath fluid (i.e., the pure suspending medium of the particle mixture) and particle mixture were each pumped through the T-shaped microchannel (see Figure 1) by an infusion syringe pump (sheath fluid, NE-300 from New Era Pump Systems, Inc.; particle suspension, KDS-100 from KD Scientific). Particle motion was visualized at the T-junction and the channel expansion (highlighted by the dashed-box in Figure 1) through an inverted microscope (Nikon Eclipse TE2000U) with a CCD camera (Nikon DS-Qi1Mc). Images were postprocessed using the Nikon imaging software (NIS-Elements AR 3.22).

DOI: 10.1021/acs.analchem.5b01432
Anal. Chem. 2015, 87, 6389−6396

THEORETICAL SECTION

Dimensionless Numbers. The dynamics of particle motion in non-Newtonian fluids through microchannels is often characterized by the following dimensionless numbers:[15,33,48] Reynolds number, Weissenberg number, and elasticity number. The Reynolds number, *Re*, is defined as the ratio of the inertial force to the viscous force,

$$Re = \frac{\rho V D_h}{\eta_0} = \frac{2\rho Q}{\eta_0 (w + h)} \tag{1}$$

where V is the average fluid velocity in the main-branch of the T-shaped microchannel (see Figure 1), $D_h = 2wh/(w + h)$ is the hydraulic diameter with w and h being the width and height of the main-branch, and Q is the volumetric flow rate through the main-branch. The Weissenberg number, *Wi*, measures the fluid elasticity effects and is defined in terms of the average shear rate, $\dot{\gamma}$, in the main-branch,

$$Wi = \lambda_e \dot{\gamma} = \lambda_e \frac{2V}{w} = \frac{2\lambda_e Q}{w^2 h} \tag{2}$$

The elasticity number, *El*, is defined as the ratio of fluid elasticity to inertia, which is independent of the flow kinematics,

$$El = \frac{Wi}{Re} = \frac{\lambda_e \eta_0 (w + h)}{\rho w^2 h} \tag{3}$$

Two other dimensionless numbers are also used in this work to study the parametric effects on particle separation via eiPFF. One is the flow rate ratio between the sheath fluid and particle mixture, α, in the two side-branches of the T-shaped microchannel, which measures the sheath flow focusing performance in the main-branch and affects the particle deflection and dispersion at the channel expansion,

$$\alpha = \frac{Q_{sheath}}{Q_{particle}} \tag{4}$$

Note that the definitions of *Re* and *Wi* in eqs 1 and 2, respectively, are both based on the total flow rate in the main-branch of the microchannel, i.e., $Q = Q_{sheath} + Q_{particle}$. The other dimensionless number is the channel aspect ratio, AR, as mentioned in the Experimental Section

$$\mathrm{AR} = w/h \tag{5}$$

which has been demonstrated to affect the equilibrium position(s) of particles in inertial microfluidics with Newtonian fluids.[15,48]

Mechanism of eiPFF. In traditional PFF,[14] particles of different sizes must first be aligned against one sidewall of the pinched branch (i.e., the main-branch of the T-shaped microchannel in Figure 1) by a strong sheath flow. This forces the centers of the particles to locate at different streamlines due to steric effects,[14,51] i.e., the center of larger particles stays further away from the wall than that of smaller ones. Subsequently, the spreading laminar flow profile at the exit of the pinched branch (i.e., the expansion of the main-branch in Figure 1) yields a continuous separation of particles based on size. For a theoretically complete separation via PFF, the maximum allowed width of the sheath flow-focused particulate solution in the main-branch, $w_{p,max}$, must fulfill (see the clarification in the Supporting Information)[52]

$$w_{p,max} = r_{p1} + r_{p2} \tag{6}$$

where r_{p1} and r_{p2} are the radii of the two types of particles to be separated. This $w_{p,max}$ corresponds to the limiting situation for which the larger particles share the same center position as those smaller particles that are most distant from the wall. Since its first introduction,[14] PFF has been improved by either reducing the particle dispersion[53] via an enhanced sheath flow focusing[54] or increasing the particle displacement via an extra force field (e.g., electrical lift,[55] inertial lift,[56] optical force,[57] and gravity[58]).

In contrast, eiPFF exploits the inherent elastic and inertial lift forces induced in a viscoelastic fluid flow to increase the lateral particle deflection for an enhanced separation. The particles to be separated need not be tightly focused, i.e., the width of the particulate solution in the main-branch can be (much) greater than the maximum allowed width, i.e., $w_{p,max}$, in eq 6 as we will demonstrate in the Results and Discussion section below. Consequently, the particle throughput in eiPFF will be significantly higher than that in the traditional PFF. Figure 2 displays the forces exerted on the particles in a viscoelastic fluid that have been focused by a sheath fluid to a layer near a sidewall. $\mathbf{F}_{eL}$ represents the elastic lift force given by[25,36]

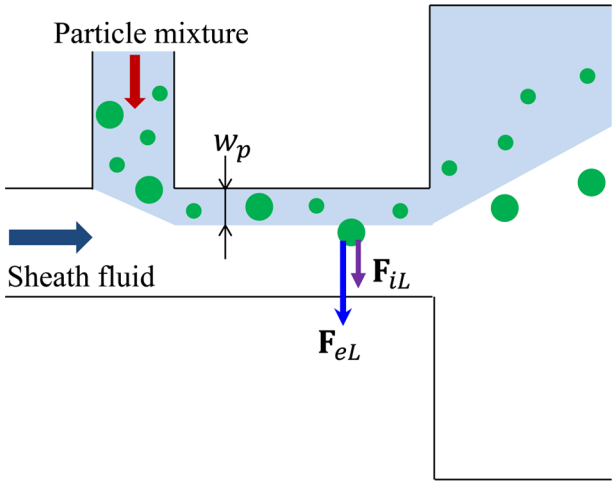

Figure 2. Schematic illustration (not to scale) of the mechanism for eiPFF. The sheath-fluid focused particle-mixture solution (highlighted by the background color) has a width of w_p in the main-branch, which for traditional PFF should be smaller than the maximum allowed width, $w_{p,max}$, given in eq 6. In eiPFF, this constraint is released because the elastic lift force, $\mathbf{F}_{eL}$, and inertial lift force, $\mathbf{F}_{iL}$, induced in a viscoelastic fluid act together to deflect particles toward the channel center at a size-dependent rate.

$$\mathbf{F}_{eL} \sim r_p^3 \nabla \mathbf{N}_1 \sim r_p^3 Wi \dot{\gamma}^2 \tag{7}$$

where r_p is the particle radius and $\mathbf{N}_1$ is the first normal stress difference. It increases with *Wi* and directs particles toward the regions of lower shear rate, i.e., the centerline and the four corners in a rectangular channel.[33] The inertial lift force, $\mathbf{F}_{iL}$, has the wall- and the shear gradient-induced components, where the former pushes particles away from the channel wall and the latter acts to direct particles toward the regions of high shear rate.[15,48] For near-wall particles, $\mathbf{F}_{iL}$ has been demonstrated to follow[59]

$$\mathbf{F}_{iL} \sim \rho V_m^2 r_p^6 / w^4 \tag{8}$$

DOI: 10.1021/acs.analchem.5b01432
Anal. Chem. 2015, 87, 6389−6396

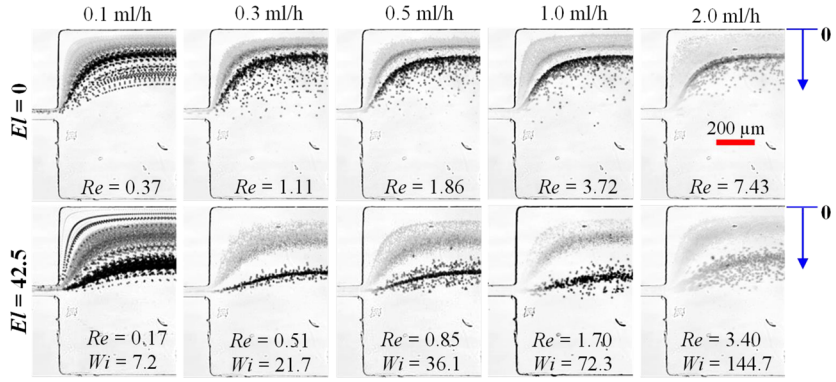

Figure 3. Superimposed images at the expansion of the main-branch comparing the continuous separation of 3 μm (appearing gray) and 10 μm (appearing black) particles in glycerol/water-based Newtonian (top row, $El = 0$) and non-Newtonian (bottom row, 1000 ppm PEO, $El = 42.5$) fluids at various sheath flow rates (indicated on top of the images) in a 40 μm deep T-shaped microchannel. The flow rate ratio between the sheath fluid and particle mixture was maintained at $\alpha = 20$. The arrows on the right-most images indicate the reference points to which the particle stream positions shown in Figures 4 and 8 were measured. The flow direction is from left to right in all images.

with V_m being the maximum fluid velocity. As indicated by the arrows in Figure 2, $\mathbf{F}_{eL}$ and $\mathbf{F}_{iL}$ work together to deflect particles toward the channel center. This is why we term this particle separation approach eiPFF, which is efficient due to the strong dependence of both types of lift forces on particle size.

RESULTS AND DISCUSSION

Effects of Fluid Elasticity (*Wi*) and Inertia (*Re*). Figure 3 shows the effects of fluid elasticity (in terms of *Wi*) and inertia (in terms of *Re*) on the continuous separation of 3 and 10 μm particles in Newtonian ($El = 0$, top row) and non-Newtonian (1000 ppm PEO with $El = 42.5$, bottom row) fluids, respectively, in a 40-μm deep channel. The flow rate ratio between the sheath fluid and particle mixture was maintained at $\alpha = 20$. A 3D numerical simulation of the flow field (COMSOL) reveals that at this ratio the particle solution is squeezed to a fluid layer with $w_p = 7$ μm (more accurately, varying from 6.5 μm in the middle plane to 7.5 μm near the top/bottom walls; see the highlighted dimension in Figure 2) in the main-branch. This value is slightly larger than the maximum allowed width of the focused particle solution, i.e., $w_{p,max} = (3.1 + 9.9)/2 = 6.5$ μm in eq 6, for the traditional PFF. In other words, the two particles cannot be completely separated by PFF at $\alpha = 20$. This analysis is consistent with the particle separation in the Newtonian fluid at $Q_{sheath} = 0.1$ mL/h in Figure 3 (top row), where both sizes of particles experience a negligible inertial lift in the main-branch at $Re = 0.37$ and still overlap with each other at the expansion. With the increase of *Re*, 10 μm particles experience a greater inertial lift and are pushed away from the wall at a visibly higher rate than 3 μm ones. An almost clear gap with only a few particles of either size present is thus formed in between the two particle streams as seen from the images at $Q_{sheath} = 0.3–1$ mL/h in Figure 3 (top row). This separation does not seem to get apparently better at flow rates higher than 1.0 mL/h ($Re = 3.72$) due to the influence of particle dispersion, which is mainly caused by the insufficient particle focusing and the parabolic fluid velocity profile in the channel depth.

In contrast, the non-Newtonian fluid yields a considerably better separation of 3 and 10 μm particles; see the bottom row images in Figure 3. This is attributed to the elasticity-enhanced deflections of both particles in the viscoelastic fluid. At the sheath flow rate $Q_{sheath} = 0.1$ mL/h, 10 μm particles seem to have an (unstable) equilibrium position near the channel wall (or more accurately, the corner) other than that along the centerline. This phenomenon is absent from 3 μm particles and happens due to the dominant elastic lift force at $Wi = 7.2$ over the inertial lift force at $Re = 0.17$, which is consistent with previous observations.[34−36] With the increase of both *Re* and *Wi* at higher flow rates, 10 μm particles migrate toward the channel centerline yielding a wide and clear gap from the stream of 3 μm particles. However, the deflection of 10 μm particles does not increase monotonically with *Re* due to the combined effects of viscoelastic and inertial lift forces, which direct particles toward the channel centerline[33−37] and the halfway (specifically 0.4 times the channel half-width from the wall),[15,48,59] respectively. It achieves the maximum at $Q_{sheath} = 1$ mL/h with $Re = 1.70$ among the tested cases in Figure 3 (bottom row), where 10 μm particles are still slightly off the channel center. This implies that the previously reported elasto-inertial particle focusing along the centerline of a straight square microchannel[36,40,45] is sensitive to the flow kinematics and works within a narrow range of flow rate.

A quantitative comparison of the exiting positions of 3 μm- and 10 μm-particle streams in the Newtonian and non-Newtonian fluids is shown in Figure 4. The data (symbols) were measured directly from the particle images in Figure 3, where the top sidewall of the channel expansion was used as the reference point (see the arrows in Figure 3) and the center of the particle traces with the lowest intensity (note the lower intensity, the darker in a gray scale image) was used as the measuring point. In the Newtonian fluid, the center position of the 3 μm particle stream changes slightly at around 80 μm (with ±50 μm error bars included in Figure 4 to cover the span of the stream) for the range of flow rates tested. This indicates that 3 μm particles remain confined within the sheath flow-focused particulate solution, which, as noted above, is about 7 μm wide in the 50 μm-wide main-branch and should become around 126 μm in the 900 μm-wide expansion due to the laminar flow feature. In the non-Newtonian fluid, however, 3 μm particles can travel out of the sheath flow-focused particulate solution due to the elastic lift force. Their deflection remains nearly unchanged at around 150 μm when $Q_{sheath} \leq 1$ mL/h ($Re = 1.7$; see Figure 3) and decreases slightly at higher flow rates. The displacement of 10 μm particles increases at a higher flow rate in the Newtonian fluid, which converges to the previously reported equilibrium position for inertial particle focusing in a (nearly) square microchannel,[15,48,59] i.e., 0.4 ×

DOI: 10.1021/acs.analchem.5b01432
Anal. Chem. 2015, 87, 6389−6396

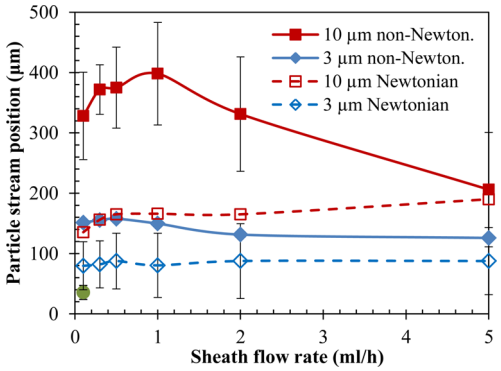

Figure 4. Comparison of the exiting positions of 3 and 10 μm particle streams at the expansion of the main-branch (measured from the images in Figure 3 with reference to the top sidewall as indicated by the arrows) in Newtonian (dashed lines with unfilled symbols) and non-Newtonian (solid lines with filled symbols) fluids. Error bars are included for only 3 μm particles in the Newtonian fluid and 10 μm particles in the non-Newtonian fluid for a nonblocked view, which encompass the span of each particle stream. The single data point with a circular symbol near the origin of the plot indicates an (unstable) equilibrium position at the corner of the channel for 10 μm particles in the non-Newtonian fluid due to the dominant elastic lift force at a negligible *Re*. Note that all lines are used to guide eyes only.

(900/2) = 180 μm. Moreover, the 10 μm particle deflection in the non-Newtonian fluid (with error bars included in Figure 4) seems to approach the same equilibrium position as in the Newtonian fluid at high flow rates. The former is, however, more than twice larger when Q_{sheath} < 2 mL/h (*Re* = 3.40) due to the dominant elasticity over inertia.

Effect of Flow Rate Ratio (α) between Sheath Fluid and Particle Mixture. The effect of flow rate ratio, α, between sheath fluid and particle mixture on particle separation via eiPFF was studied in 1000 ppm PEO solution by fixing the sheath flow rate at Q_{sheath} = 0.3 mL/h while varying the particle flow rate from 90 μL/h (i.e., α = 3.3) to 6 μL/h (i.e., α = 50) in a 40 μm deep T-shaped microchannel. Figure 5 shows the superimposed images of 3 and 10 μm particles at the T-junction (top row) and expansion (bottom row) of the main-branch, which clearly demonstrate an enhanced particle separation with the increase of α. Since the total flow rate in the main-branch does not change significantly, *Re* (labeled on the images in Figure 5) slightly decreases from 0.63 to 0.50 when α (as labeled on the images) increases from 3.3 to 50. Accordingly, *Wi* also decreases slightly to maintain the elasticity number at *El* = 42.5. These indicate nearly constant inertial and elastic effects for the cases tested in Figure 5, which explains why the average deflections of 3 and 10 μm particles at the expansion remain nearly unaffected by the change of α (see the two dotted lines across the images in the bottom row).

However, as viewed from the images at the T-junction in Figure 5 (top row), the particle mixture solution is squeezed by the sheath fluid to a narrower layer in the main-branch with the increase of α. This enhanced focusing helps aligning both sizes of particles, especially important for the smaller ones, against the channel wall, leading to a smaller band of each particle type at the expansion (see the bottom row images in Figure 5). Our 3D flow simulation (COMSOL) tells that the width of the sheath flow-focused particulate solution, i.e., w_p as highlighted in Figure 2, decreases from 15.1 μm to 13.0, 9.9, 7.4, and 5.5 μm for the tested values of α at 3.3, 5, 10, 20, and 50 in Figure 5. The first five width values are all greater than the maximum allowed width, i.e., $w_{p,max}$ = 6.5 μm, for a theoretically 100% separation via PFF. As a decent separation can be achieved at α as low as 5, eiPFF is able to offer a much higher particle throughput than PFF (which works only for α > 30 based on our 3D flow simulation) at the same sheath flow rate.

Effect of PEO Concentration (In Terms of *El*). Figure 6 shows the effect of PEO concentration on the separation of 3 and 10 μm particles via eiPFF in a 40 μm deep T-shaped microchannel. The sheath flow rate, Q_{sheath}, was varied to include the inertial effect, but the flow rate ratio was maintained at α = 20. Three different PEO concentrations were tested, which are 500, 1000, and 2000 ppm. As the fluid viscosity and relaxation time (see Table 1) both increase at a higher PEO concentration, *Re* (labeled on the images) decreases while *Wi* increases yielding a significantly increasing *El* as highlighted in Figure 6. To assist viewing the concentration effect on the particle stream positions, dotted lines, which indicate the exiting positions of 3 and 10 μm particles in 1000 ppm PEO solution (*El* = 42.5), have been added onto the images in Figure 6. For the range of flow rates tested (up to Q_{sheath} = 5 mL/h), 3 μm particles attain a larger deflection with the increase of PEO concentration due to a stronger elastic lift force. Their trajectories, however, do not change significantly with *Re*, except in 2000 ppm PEO solution. These behaviors are better viewed from the exiting stream positions in Figure 7. The deflection of 3 μm particles in 2000 ppm PEO solution quickly decreases from around 260 to 100 μm with the increase of flow

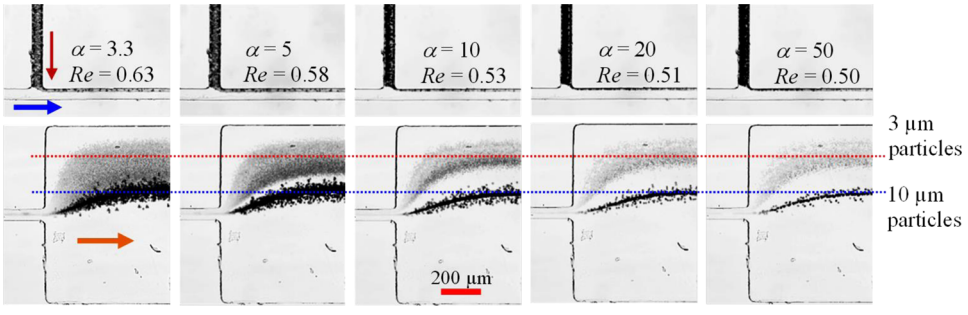

Figure 5. Superimposed images at the T-junction (top row) and expansion (bottom row) of the main-branch illustrating the sheath-flow focusing and elasto-inertial separation of 3 and 10 μm particles in 1000 ppm PEO solution through a 40 μm deep T-shaped microchannel. The volume flow rate of the sheath fluid, Q_{sheath}, was maintained at 0.3 mL/h in all cases. The flow rate ratio between the sheath fluid and particle mixture, α, was varied as seen on the images. The two dotted lines across the images are used to assist viewing the effects of α on the exiting positions of the separated particle streams. The block arrows indicate the flow directions.

DOI: 10.1021/acs.analchem.5b01432
Anal. Chem. 2015, 87, 6389−6396

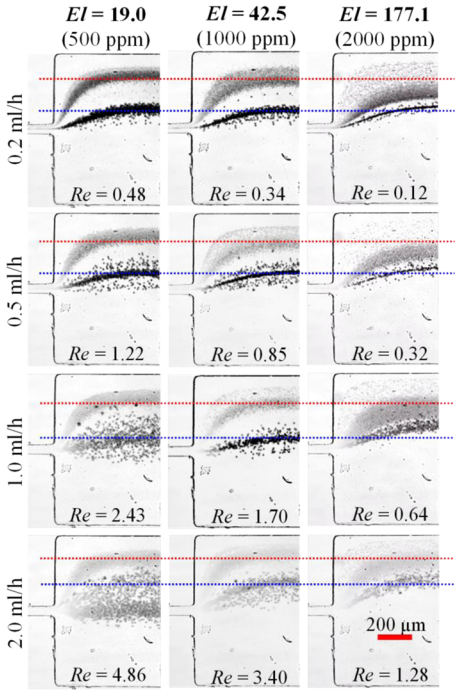

Figure 6. Superimposed images at the expansion of the main-branch illustrating the effect of PEO concentration (500, 1000, and 2000 ppm from left to right; in terms of *El*) on the separation of 3 and 10 μm particles via eiPFF in a 40 μm deep T-shaped microchannel. The flow rate ratio between sheath fluid (labeled to the left of the images) and particle mixture was fixed at 20. The dotted lines across the images, which indicate the exiting positions of the two types of particles in 1000 ppm PEO solution, are drawn to assist viewing the PEO concentration effect on the particle stream positions at the expansion.

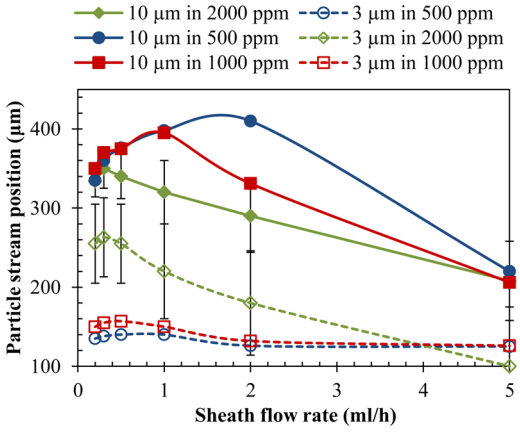

Figure 7. Comparison of the exiting positions of 3 μm (dashed lines) and 10 μm (solid lines) particle streams at the expansion of the main-branch (measured directly from the images in Figure 6) in non-Newtonian fluids with different PEO concentrations. Error bars are included for particles suspended in 2000 ppm PEO solution. Note that all lines are used to guide the eyes only.

rate. This phenomenon is believed to be a consequence of the shear thinning effect that gets stronger at a higher PEO concentration and tends to move particles away from the channel centerline.[31,32]

In contrast, the deflection of 10 μm particles is much more profound and dependent on both *Re* and *El* (or *Wi*). It attains the maximum value in 1000 ppm PEO solution at small flow rates (up to 1 mL/h) while in 500 ppm PEO solution at higher flow rates. Since 3 μm particles experience a larger deflection at a higher PEO concentration, the separation in 2000 ppm PEO turns out to be the worst in all tested flow rates as seen from Figure 6. This is clearly viewed from the exiting positions of both particle streams (with error bars included to cover the span) in Figure 7. The 10 μm particle deflection follows a similar first-rise/then-drop trend with *Re* in all three PEO solutions. However, the turning point occurs at the largest flow rate in 500 ppm PEO (2 mL/h vs 1 mL/h in 1000 ppm and 0.3 mL/h in 2000 ppm. Interestingly and importantly, 10 μm particles can be deflected all the way to the channel center in 500 ppm PEO solution, which was not observed in the two higher concentrations. This may imply a potentially high-throughput particle separation in a low concentration PEO solution or a non-Newtonian fluid with a weaker elasticity such as the hyaluronic acid used recently for inertia-elastic particle focusing at *Re* up to 10 000.[39]

Effect of Channel Aspect Ratio (AR). Figure 8 shows the effect of channel aspect ratio, AR, on the separation of 3 and 10 μm particles via eiPFF in 1000 ppm PEO solution through 100, 40, and 25 μm (from left to right) deep T-shaped microchannels. Both *Re* and *Wi* increase in a shallower channel, i.e., with a larger AR, while the latter is about twice as fast. This yields an increasing *El* with the increase of AR. In the channel with AR = 0.5 (i.e., 100 μm deep), 10 μm particles can have two equilibrium positions, i.e., the corners and centerline, at Q_{sheath} < 0.3 mL/h in Figure 8 (left column) due to the dominant elastic lift force at negligible *Re*. Moreover, the higher the flow rate, the more 10 μm particles are along the centerline. This phenomenon is different from the inertial particle motion in Newtonian fluids in a low-AR microchannel, where the

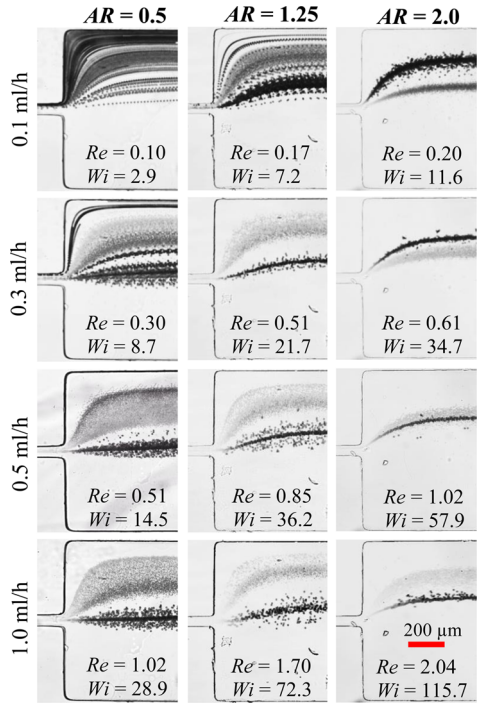

Figure 8. Superimposed images at the expansion of the main-branch illustrating the effect of aspect ratio, AR, on the 3 and 10 μm particle separation via eiPFF in T-shaped microchannels of various depths (100, 40, and 25 μm from left to right). The sheath flow rate, Q_{sheath}, was varied as labeled while the flow rate ratio between sheath fluid and particle mixture was fixed at 20.

DOI: 10.1021/acs.analchem.5b01432
Anal. Chem. 2015, 87, 6389−6396

particle equilibrium positions are preferably centered at the wider faces in the channel depth direction.[15,48,60] A visible separation of 10 μm particles from 3 μm particles is achieved at Q_{sheath} = 0.5 mL/h (Re = 0.51) and gets better at 1.0 mL/h. This trend is similar to that in the channel with AR = 1.25 (i.e., 40 μm deep, middle column of Figure 8) where the separation is visually better though the deflections of both sizes of particles are smaller. In contrast, the particle behavior in the channel with AR = 2.0 (i.e., 25 μm deep) are much more interesting. As seen from the images in the right column of Figure 8, the deflection of 10 μm particles can be either smaller (at low flow rates) or larger (at high flow rates) than that of 3 μm particles depending on the value of Re. This switch takes place at Q_{sheath} = 0.5 mL/h where Re = 1.02. Such a surprising phenomenon also occurs for 500 and 2000 ppm PEO solutions in the same channel (data not shown). It is, however, absent from the particle motion in Newtonian fluids, where larger particles always migrate to the channel centerline faster than smaller ones due to the rotation-induced inertial lift force.[61] In addition, the stream width of each size of particles in the 25 μm deep channel seems to be the narrowest among the three channels due to perhaps the strongest steric effects from the top/bottom walls therein.

Figure 9 compares the exiting positions of 3 and 10 μm particle streams (with error bars included) at the expansion of the main-branch in T-shaped microchannels with (A) AR = 0.5 (i.e., 100 μm deep) and (B) AR = 2.0 (i.e., 25 μm deep), respectively. These two graphs can be compared directly to that in Figure 4 for the channel with AR = 1.25 (i.e., 40 μm deep). The deflection of 10 μm particles exhibits a similar trend in all three depths of channels, which first increases with the rise of flow rate and then decreases at higher flow rates. However, the maximum deflection decreases from 450 μm (right along the centerline of the expansion) in the deepest channel to around 340 μm in the shallowest channel. While the flow rate at which the maximum particle deflection happens seems to remain at approximately 1 mL/h in all three channels, the slope of the decreasing particle deflection with flow rate turns out to be the steepest in the 40 μm deep channel. In contrast, the deflection of 3 μm particles in the 25 μm-deep channel decreases with the increase of flow rate, which is apparently different from that in the two deeper channels.

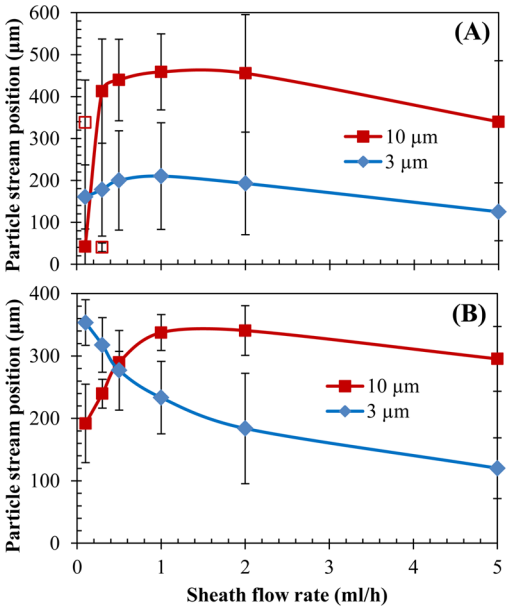

Figure 9. Comparison of the exiting positions (symbols with error bars, measured directly from the images in Figure 8) of 3 and 10 μm particle streams in 1000 ppm PEO solution at the expansion of the main-branch in T-shaped microchannels with (A) AR = 0.5 (100 μm deep) and (B) AR = 2.0 (25 μm deep), respectively. The unfilled data points in (A) represent a secondary equilibrium position (with fewer particles present) at the corner of the channel for 10 μm particles. Note that all lines are used to guide the eyes only.

CONCLUSIONS

We have conducted a systematic experimental study of the continuous particle separation in PEO solutions via eiPFF. Five dimensionless numbers, i.e., Re, Wi, El, α, and AR, have been used to quantify the parametric effects for a fundamental understanding of the important factors in device design and control. We have demonstrated that eiPFF offers a much higher particle throughput and a much better separation resolution than the traditional PFF. Moreover, as it works most efficiently for Re of order 1, eiPFF fills perfectly into the gap of our recently proposed inertia-enhanced PFF (iPFF) technique[56] that requires Re of order 10 or more. This feature makes eiPFF suitable for particle and cell separation in microfluidic devices that typically process a limited amount of samples.[62,63] In addition, eiPFF has the potential to separate particles of 1 μm diameter[26] or even smaller,[34] which is very hard (if not impossible) for iPFF[56] and other inertia-based separation techniques.[15,48] We have also observed two new phenomena that have not been reported in the literature: one is that the particle focusing and separation via eiPFF does not increase monotonically with El at higher PEO concentrations due to the mutual influences of elastic and inertial effects; and the other is that the channel aspect ratio, AR, strongly affects the particle separation due to its influence on the particle deflection. More surprisingly, the elasto-inertial deflection of small particles can be even greater than that of large ones in a high-AR channel when Re is less than 1.

ASSOCIATED CONTENT

Supporting Information

Details on how to determine the Newtonian and non-Newtonian fluid properties in Table 1 and how to understand eq 6. The Supporting Information is available free of charge on the ACS Publications website at DOI: 10.1021/acs.analchem.5b01432.

AUTHOR INFORMATION

Corresponding Author

*E-mail: xcxuan@clemson.edu. Fax: +1 864 656 5630. Phone: +1 864 656 7299.

Notes

The authors declare no competing financial interest.

ACKNOWLEDGMENTS

This work was partially supported by Clemson University through a departmental SGER (Small Grants for Exploratory Research) grant.

REFERENCES

(1) Pamme, N. *Lab Chip* **2007**, *7*, 1644–1659.

DOI: 10.1021/acs.analchem.5b01432
Anal. Chem. 2015, 87, 6389–6396

(2) Gossett, D. R.; Weaver, W. M.; Mach, A. J.; Hur, S. C.; Tse, H. T.; Lee, W.; Amini, H.; Di Carlo, D. *Anal. Bioanal. Chem.* **2010**, *397*, 3249−3267.
(3) Karimi, A.; Yazdi, S.; Ardekani, A. M. *Biomicrofluidics* **2013**, *7*, 021501.
(4) Pethig, R. *Biomicrofluidics* **2010**, *4*, 022811.
(5) Kim, S. B.; Yoon, S. Y.; Sung, H. J.; Kim, S. S. *Anal. Chem.* **2008**, *80*, 2628−2630.
(6) Ding, X.; Li, P.; Lin, P. S. C.; Stratton, Z. S.; Nama, N.; Guo, F.; Slotcavage, D.; Mao, X.; Shi, J.; Costanzo, F.; Huang, T. J. *Lab Chip* **2013**, *13*, 3626−3649.
(7) Hejazian, M.; Li, W.; Nguyen, N. T. *Lab Chip* **2015**, *15*, 959−970.
(8) Watarai, H. *Annu. Rev. Anal. Chem.* **2013**, *6*, 353−378.
(9) Regtmeier, J.; Eichhorn, R.; Viefhues, M.; Bogunovic, L.; Anselmetti, D. *Electrophoresis* **2011**, *32*, 2253−2273.
(10) Huang, L.; Cox, E. C.; Austin, R. H.; Sturm, J. C. *Science* **2004**, *304*, 987−990.
(11) Yamada, M.; Seki, M. *Anal. Chem.* **2006**, *78*, 1357−1362.
(12) Choi, S. Y.; Song, S.; Choi, C.; Park, J. K. *Anal. Chem.* **2009**, *81*, 1964−1968.
(13) Giddings, J. C. *J. Chromatogr.* **1989**, *480*, 21−33.
(14) Yamada, M.; Nakashima, M.; Seki, M. *Anal. Chem.* **2004**, *76*, 5465−5471.
(15) Martel, J. M.; Toner, M. *Annu. Rev. Biomed. Eng.* **2014**, *16*, 371−396.
(16) Pipe, C. J.; McKinley, G. H. *Mech. Res. Commun.* **2009**, *36*, 110−120.
(17) Berli, C. L. A. *Electrophoresis* **2013**, *34*, 622−630.
(18) Zhao, C.; Yang, C. *Adv. Colloid Interface Sci.* **2013**, *201−202*, 94−108.
(19) Karnis, A.; Goldsmith, H. L.; Mason, S. G. *Nature* **1963**, *200*, 159−160.
(20) Karnis, A.; Mason, S. G. *Trans. Soc. Rheol.* **1966**, *10*, 571−592.
(21) McKinley, G. H. *Transport Processes in Bubbles, Drops & Particles*, 2nd ed.; Chhabra, R.; D. De Kee, Eds.; Taylor & Francis: New York, 2002; Chapter 14.
(22) Leal, G. *J. Non-Newton. Fluid Mech.* **1979**, *5*, 33−78.
(23) Becker, L. E.; McKinley, G. H.; Rasmussen, H. K.; Hassager, O. *J. Rheol.* **1994**, *38*, 377−403.
(24) Arigo, M. T.; Mckinley, G. H. *Rheol. Acta* **1998**, *37*, 307−327.
(25) Leshansky, A. M.; Bransky, A.; Korin, N.; Dinnar, U. *Phys. Rev. Lett.* **2007**, *98*, 234501.
(26) Kang, K.; Lee, S. S.; Hyun, K.; Lee, S. J.; Kim, J. M. *Nat. Commun.* **2013**, *4*, No. 2567, DOI: 10.1038/ncomms3567.
(27) Romeo, G.; D'Avino, G.; Greco, F.; Nettiab, P. A.; Maffettone, P. L. *Lab Chip* **2013**, *13*, 2802−2807.
(28) Ho, B. P.; Leal, L. G. *J. Fluid Mech.* **1976**, *76*, 783−799.
(29) Huang, P. Y.; Feng, J.; Hu, H. H.; Joseph, D. D. *J. Fluid Mech.* **1997**, *343*, 73−94.
(30) Villone, M. M.; D'Avino, G.; Hulsen, M. A.; Greco, F.; Maffettone, P. L. *J. Non-Newton. Fluid Mech.* **2011**, *166*, 1396−1405.
(31) Huang, P. Y.; Joseph, D. D. *J. Non-Newton. Fluid Mech.* **2000**, *90*, 159−185.
(32) Seo, K. W.; Byeon, H. J.; Huh, H. K.; Lee, S. J. *RSC Adv.* **2014**, *4*, 3512−3520.
(33) D'Avino, G.; Maffettone, P. L. *J. Non-Newton. Fluid Mech.* **2015**, *215*, 80−104.
(34) Kim, J. Y.; Ahn, S. W.; Lee, S. S.; Kim, J. M. *Lab Chip* **2012**, *12*, 2807−2814.
(35) Seo, K. W.; Kang, Y. J.; Lee, S. J. *Phys. Fluid.* **2014**, *26*, 063301.
(36) Yang, S. Y.; Kim, J. Y.; Lee, S. J.; Lee, S. S.; Kim, J. M. *Lab Chip* **2011**, *11*, 266−273.
(37) Giudice, F. D.; Romeo, G.; D'Avino, G.; Greco, F.; Netti, P. A.; Maffettone, P. L. *Lab Chip* **2013**, *13*, 4263−4271.
(38) Lim, H.; Nam, J.; Shin, S. *Microfluid. Nanofluid.* **2014**, *17*, 683−692.
(39) Lim, E. J.; Ober, T.; Edd, J. F.; Desai, S. P.; Neal, D.; Bong, K. W.; Doyle, P. S.; McKinley, G. H.; Toner, M. *Nat. Commun.* **2014**, *5*, No. 4120, DOI: 10.1038/ncomms5120.
(40) Ahn, S. W.; Lee, S. S.; Lee, S. J.; Kim, J. M. *Chem. Eng. Sci.* **2015**, *126*, 237−243.
(41) Cha, S.; Kang, K.; You, J. B.; Im, S. G.; Kim, Y.; Kim, J. M. *Rheol. Acta* **2014**, *53*, 927−933.
(42) Lee, D. L.; Brenner, H.; Youn, J. R.; Song, Y. S. *Sci. Rep.* **2013**, *3*, No. 3258, DOI: 10.1038/srep03258.
(43) Cha, S.; Shin, T.; Lee, S. S.; Shim, W.; Lee, G.; Lee, S. J.; Kim, Y.; Kim, J. M. *Anal. Chem.* **2012**, *84*, 10471−10477.
(44) Seo, K. W.; Ha, Y. R.; Lee, S. J. *Appl. Phys. Lett.* **2014**, *104*, 213702.
(45) Yang, S.; Lee, S. S.; Ahn, S. W.; Kang, K.; Shim, W.; Lee, G.; Hyune, K.; Kim, J. M. *Soft Matter* **2012**, *8*, 5011−5019.
(46) Geislinger, T. M.; Franke, T. *Adv. Colloid Interface Sci.* **2014**, *208*, 161−176.
(47) Nam, J.; Lim, H.; Kim, D.; Jung, H.; Shin, S. *Lab Chip* **2012**, *12*, 1347−1354.
(48) Amini, H.; Lee, W.; Di Carlo, D. *Lab Chip* **2014**, *14*, 2739−2761.
(49) Liang, L.; Qian, S.; Xuan, X. *J. Colloid Interface Sci.* **2010**, *350*, 377−379.
(50) Lu, X.; Patel, S.; Zhang, M.; Joo, S.; Qian, S.; Ogale, A.; Xuan, X. *Biomicrofluids* **2014**, *8*, 021802.
(51) Maenaka, H.; Yamada, M.; Yasuda, M.; Seki, M. *Langmuir* **2008**, *24*, 4405−4410.
(52) Mortensen, N. A. *Anal. Chem.* **2007**, *79*, 9240−9241.
(53) Jain, A.; Posner, J. D. *Anal. Chem.* **2008**, *80*, 1641−1648.
(54) Nho, H. W.; Yoon, T. H. *Lab Chip* **2013**, *13*, 773−776.
(55) Lu, X.; Hsu, J. P.; Xuan, X. *Langmuir* **2015**, *31*, 620−627.
(56) Lu, X.; Xuan, X. *Anal. Chem.* **2015**, *87*, 4560−4565.
(57) Lee, K. H.; Kim, S. B.; Lee, K. S.; Sung, H. J. *Lab Chip* **2011**, *11*, 354−357.
(58) Morijiri, M.; Sunahiro, S.; Senaha, M.; Yamada, M.; Seki, M. *Microfluid. Nanofluid.* **2011**, *11*, 105−110.
(59) Di Carlo, D.; Edd, J. F.; Humphry, K. J.; Stone, H. A.; Toner, M. *Phys. Rev. Lett.* **2009**, *102*, 094503.
(60) Bhagat, A. A. S.; Kuntaegowdanahalli, S. S.; Papautsky, I. *Phys. Fluid.* **2008**, *20*, 101702.
(61) Zhou, J.; Papautsky, I. *Lab Chip* **2013**, *13*, 1121−1132.
(62) Reyes, D. R.; Iossifidis, D.; Auroux, P. A.; Manz, A. *Anal. Chem.* **2002**, *74*, 2623−2636.
(63) Auroux, P. A.; Iossifidis, D.; Reyes, D. R.; Manz, A. *Anal. Chem.* **2002**, *74*, 2627−2652.

DOI: 10.1021/acs.analchem.5b01432
Anal. Chem. 2015, 87, 6389−6396